JCI insight

Long noncoding RNA Malat1 regulates differential activation of macrophages and response to lung injury

Huachun Cui, … , Victor J. Thannickal, Gang Liu

Research Article   Immunology   Pulmonology

Macrophage activation, i.e., classical M1 and the alternative M2, plays a critical role in many pathophysiological processes, such as inflammation and tissue injury and repair. Although the regulation of macrophage activation has been under extensive investigation, there is little knowledge about the role of long noncoding RNAs (lncRNAs) in this event. In this study, we found that lncRNA Malat1 expression is distinctly regulated in differentially activated macrophages in that it is upregulated in LPS-treated and downregulated in IL-4–treated cells. Malat1 knockdown attenuates LPS-induced M1 macrophage activation. In contrast, Malat1 knockdown enhanced IL-4–activated M2 differentiation as well as a macrophage profibrotic phenotype. Mechanistically, Malat1 knockdown led to decreased expression of Clec16a, silencing of which phenocopied the regulatory effect of Malat1 on M1 activation. Interestingly, Malat1 knockdown promoted IL-4 induction of mitochondrial pyruvate carriers (MPCs) and their mediation of glucose-derived oxidative phosphorylation (OxPhos), which was crucial to the Malat1 regulation of M2 differentiation and profibrotic phenotype. Furthermore, mice with either global or conditional myeloid knockout of Malat1 demonstrated diminished LPS-induced systemic and pulmonary inflammation and injury. In contrast, these mice developed more severe bleomycin-induced lung fibrosis, accompanied by alveolar macrophages displaying augmented M2 and profibrotic phenotypes. In summary, we have identified what we believe is a previously unrecognized role of Malat1 in the regulation of macrophage polarization. Our data demonstrate that Malat1 […]

Find the latest version:

https://jci.me/124522/pdf

Long noncoding RNA Malat1 regulates differential activation of macrophages and response to lung injury

Huachun Cui,[1] Sami Banerjee,[1] Sijia Guo,[1,2] Na Xie,[1] Jing Ge,[1,3] Dingyuan Jiang,[1,4] Martin Zörnig,[5] Victor J. Thannickal,[1] and Gang Liu[1]

[1]Division of Pulmonary, Allergy, and Critical Care Medicine, Department of Medicine, University of Alabama at Birmingham, Birmingham, Alabama, USA. [2]Department of Pulmonary, Allergy, and Critical Care Medicine, The Second Affiliated Hospital, Tianjin University of Traditional Chinese Medicine, Tianjin, China. [3]Department of Geriatrics and Institute of Geriatrics, Union Hospital, Tongji Medical College, Huazhong University of Science and Technology, Wuhan, China. [4]Department of Pulmonary and Critical Care Medicine, Center of Respiratory Medicine, China-Japan Friendship Hospital, National Clinical Research Center for Respiratory Diseases, Beijing, China. [5]Georg-Speyer-Haus, Institute for Tumor Biology and Experimental Therapy, Frankfurt, Germany.

Macrophage activation, i.e., classical M1 and the alternative M2, plays a critical role in many pathophysiological processes, such as inflammation and tissue injury and repair. Although the regulation of macrophage activation has been under extensive investigation, there is little knowledge about the role of long noncoding RNAs (lncRNAs) in this event. In this study, we found that lncRNA Malat1 expression is distinctly regulated in differentially activated macrophages in that it is upregulated in LPS-treated and downregulated in IL-4–treated cells. Malat1 knockdown attenuates LPS-induced M1 macrophage activation. In contrast, Malat1 knockdown enhanced IL-4– activated M2 differentiation as well as a macrophage profibrotic phenotype. Mechanistically, Malat1 knockdown led to decreased expression of Clec16a, silencing of which phenocopied the regulatory effect of Malat1 on M1 activation. Interestingly, Malat1 knockdown promoted IL-4 induction of mitochondrial pyruvate carriers (MPCs) and their mediation of glucose-derived oxidative phosphorylation (OxPhos), which was crucial to the Malat1 regulation of M2 differentiation and profibrotic phenotype. Furthermore, mice with either global or conditional myeloid knockout of Malat1 demonstrated diminished LPS-induced systemic and pulmonary inflammation and injury. In contrast, these mice developed more severe bleomycin-induced lung fibrosis, accompanied by alveolar macrophages displaying augmented M2 and profibrotic phenotypes. In summary, we have identified what we believe is a previously unrecognized role of Malat1 in the regulation of macrophage polarization. Our data demonstrate that Malat1 is involved in pulmonary pathogeneses in association with aberrant macrophage activation.

Introduction

Macrophages constitute an essential element of innate and adaptive immune systems. These cells display remarkable phenotypic diversity that is largely dictated by their activation status (1, 2). Macrophages that are activated by IFN-γ and/or TLR ligands have been historically called M1 or classically activated macrophages, and those activated by IL-4/IL-13, immune complexes plus TLR ligands, IL-10, TGF-β, or glucocorticoids are often referred to as M2 or alternatively activated macrophages (1, 3–7). However, there is a recent proposal for a new nomenclature linked to the type of activators to better reflect the phenotypic origins and to improve experimental standardization (8).

While M1 macrophages produce high amounts of proinflammatory cytokines and are critical to the eradication of bacterial, viral, and fungal infections (1–3), M2 macrophages play an important role in host response to parasite infection, tissue remodeling, angiogenesis, and tumor progression (1, 2, 9). The regulation of macrophage activation has been extensively studied, particularly at transcriptional and epigenetic levels, as dysregulation of this process is profoundly associated with numerous pathologies (1, 7). Recently, there has been rapidly growing interest in the role of a new class of molecules, noncoding RNAs

(ncRNAs), in these regulatory events. While there is plenty of evidence showing that small ncRNAs, such as microRNAs (miRs), participate in macrophage activation by targeting various mediators (10, 11), it remains far less clear if, or how, long ncRNAs (lncRNAs) regulate this process.

In our continuing effort to characterize ncRNAs in macrophage activation, we found that metastasis-associated lung adenocarcinoma transcript 1 (Malat1), a lncRNA previously shown to have a critical regulatory function in lung cancer metastasis and cell migration (12–14), has a unique role in this process in that it promotes M1 and inhibits M2 macrophage polarization. Malat1 expression is distinctly regulated in macrophages in the 2 polarized states. More importantly, we found that Malat1 participates in the pathogeneses of pulmonary disorders that definitively involve differential activation of lung macrophages.

Results

Malat1 expression undergoes distinct alteration in differentially activated macrophages. To determine the role of Malat1 in macrophage activation, we initially examined the regulation of its expression by LPS and IL-4, which are classically used to induce the 2 polarized states of macrophages (4). As shown in Figure 1A, Malat1 expression started to rise as early as 4 hours after LPS treatment in mouse bone marrow–derived macrophages (BMDMs) and the elevation persisted for at least 24 hours. Malat1 was also induced in human peripheral blood mononuclear cell–derived (PBMC-derived) and human monocytic line THP-1–derived macrophages, although at a later time point after LPS treatment (Figure 1, B and C). To further characterize the regulation of Malat1 expression, we performed ChIP assays and found that NF-κB subunit p65 bound to the *Malat1* promoter in LPS-treated macrophages (Figure 1D), indicative of Malat1 being a direct transcriptional target of LPS-induced NF-κB activation. In contrast to its elevation in LPS-treated cells, Malat1 expression was inhibited by IL-4 in macrophages (Figure 1E). Taken together, our results showing that the distinct regulation of Malat1 expression by LPS and IL-4 suggest that Malat1 may participate in the differential activation of macrophages. To shed light on a mechanism underlying any potential function of Malat1 in macrophages, we determined the intracellular localization of this lncRNA by performing cell fractionation. As expected, the protein-coding tubulin α1 mRNA and the small nucleolar RNA Sno-142 were found almost exclusively in the macrophage cytoplasm and nucleus, respectively, confirming the purity of the 2 cellular fractions (Figure 1F). We found that Malat1 was predominantly localized in the macrophage nuclei (Figure 1G). Furthermore, the predominant nuclear localization remained unchanged in LPS- or IL-4–treated macrophages (Figure 1G), indicating the mechanistic site of Malat1 in these cells.

Malat1 knockdown attenuates proinflammatory activation of macrophages. To investigate if Malat1 regulates proinflammatory activation, we transfected macrophages with control or specific Malat1 GapmeRs, followed by stimulation with LPS. GapmeRs are single-stranded antisense oligonucleotides that can potently degrade complementary RNA targets via an RNase H–dependent mechanism (15, 16). We first confirmed that Malat1 GapmeRs were remarkably effective to knock down this lncRNA in macrophages (Figure 2A). More importantly, we found that Malat1 knockdown decreased LPS-induced expression of proinflammatory cytokines TNF-α, IL-6, and IL-12 at both mRNA and protein levels in macrophages (Figure 2, B and C). Consistent with the diminished production of these cytokines, LPS-treated macrophages with Malat1 knockdown also demonstrated reduced bactericidal activity (Figure 2D), a characteristic of M1 activation (1). These data, together with the finding that Malat1 was induced by LPS, suggest that Malat1 functions in a positive feedback manner to potentiate the proinflammatory response in macrophages. Of note, Malat1 has been shown to be cleaved in the nucleus by RNase P to produce a small (~60-nucleotide) cytoplasmic RNA called Malat1-associated small cytoplasmic RNA (mascRNA) (17). Although the function of mascRNA remains elusive, there are recent reports showing that it has an immune-regulatory role in cardiovascular disorders (18, 19). To determine if knockdown of Malat1 also affected mascRNA, we examined its level in the cytoplasm of Malat1-knockdown cells and found that Malat1 knockdown also led to a decrease in mascRNA level, although to a lesser extent (data not shown). These data add another layer of complexity to the Malat1 regulation of proinflammatory activation in macrophages.

Malat1 regulates the expression of Clec16a, which is required for the proinflammatory activation of macrophages. We had shown that Malat1 promoted the proinflammatory M1 macrophage activation. We then strove to delineate the underlying mechanism. Initially, we investigated if Malat1 participated in the proximal signaling cascade upon the engagement of LPS with its receptor, as it had been well known to be subject to a variety of regulations. These signaling events include LPS-induced phosphorylation of IκB-α and p65 as well as the ensuing p65 nuclear translocation (20). However, we found that Malat1 knockdown had no obvious
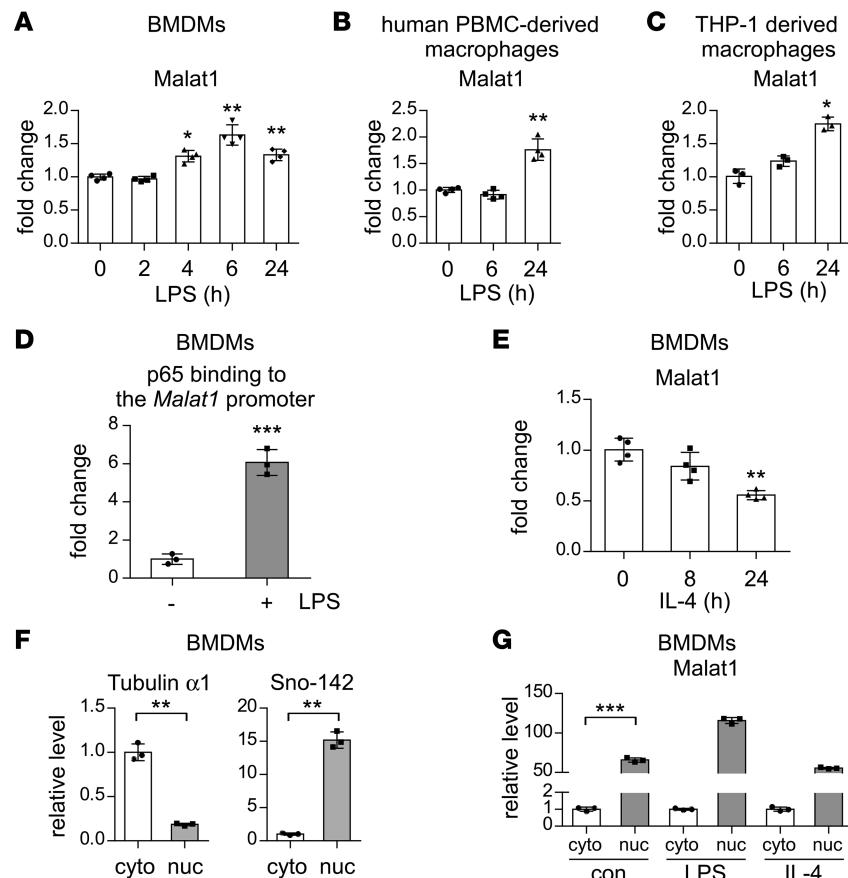
Figure 1. lncRNA Malat1 expression undergoes distinct alteration in differentially activated macrophages. (**A**) Mouse BMDMs were treated with 100 ng/ml LPS for the indicated duration of time. Total RNAs were isolated and levels of Malat1 determined by real-time PCR. $n = 4$; mean ± SD; *$P < 0.05$, **$P < 0.01$ compared with time "0". (**B**) Human PBMC-derived macrophages were treated with 100 ng/ml LPS for the indicated duration of time. Levels of Malat1 were determined. $n = 4$; mean ± SD; **$P < 0.01$ compared with time "0". (**C**) Human THP-1–derived macrophages were treated with 100 ng/ml LPS for the indicated duration of time. Levels of Malat1 were determined. $n = 3$; mean ± SD; *$P < 0.05$ compared with time "0". (**D**) BMDMs were treated with or without 100 ng/ml LPS for 1 hour. ChIP assay was performed. Levels of p65 binding to the *Malat1* promoter were determined by real-time PCR. $n = 3$; mean ± SD; ***$P < 0.001$ compared with "–LPS". (**E**) BMDMs were treated with 5 ng/ml mouse IL-4 for the indicated duration of time. Levels of Malat1 were determined. $n = 4$; mean ± SD; **$P < 0.01$ compared with time "0". (**F** and **G**) BMDMs were treated with or without 100 ng/ml LPS for 6 hours or 5 ng/ml IL-4 for 24 hours. Cell fractionation was performed, and RNAs in the cytoplasmic and nuclear fractions were isolated. Levels of tubulin α1 and Sno-142 (**F**), and Malat1 (**G**) in each fraction were determined by real-time PCR. $n = 3$; mean ± SD; **$P < 0.01$, ***$P < 0.001$. Two-tailed Student's *t* test was used (**A**–**G**) to analyze statistical significance. Representative of 2 to 3 independent experiments.

effect on the proximal signaling events in LPS-treated macrophages (Supplemental Figure 1, A and B; supplemental material available online with this article; https://doi.org/10.1172/jci.insight.124522DS1), suggesting that Malat1 does not have a role in the cytoplasm, a notion that is in concordance with this lncRNA being primarily localized in the nucleus (Figure 1G). This finding also indicates that the exclusively cytoplasmic mascRNA has no impact on the LPS-induced signaling cascade either.

The apparent lack of effect of Malat1 knockdown on the LPS-activated proximal signaling cascade as well as the predominantly nuclear localization of this lncRNA prompted us to hypothesize that Malat1 transcriptionally regulates the expression of mediators participating in the proinflammatory activation of macrophages. To identify potential transcriptional targets, we performed RNA sequencing (RNA-seq) analysis on macrophages transfected with control or Malat1 GapmeRs (GSE106913). We found dozens of genes that showed greater than 2-fold changes in expression (Supplemental Table 1). Among those, C-type lectin domain family 16, member A (Clec16a) demonstrated the greatest decrease in transcription in Malat1-knockdown cells.

Relatively little is currently known about the function of Clec16a. However, the *Clec16a* gene locus has been frequently implicated in type 1 diabetes mellitus (T1DM), multiple sclerosis, and other forms of
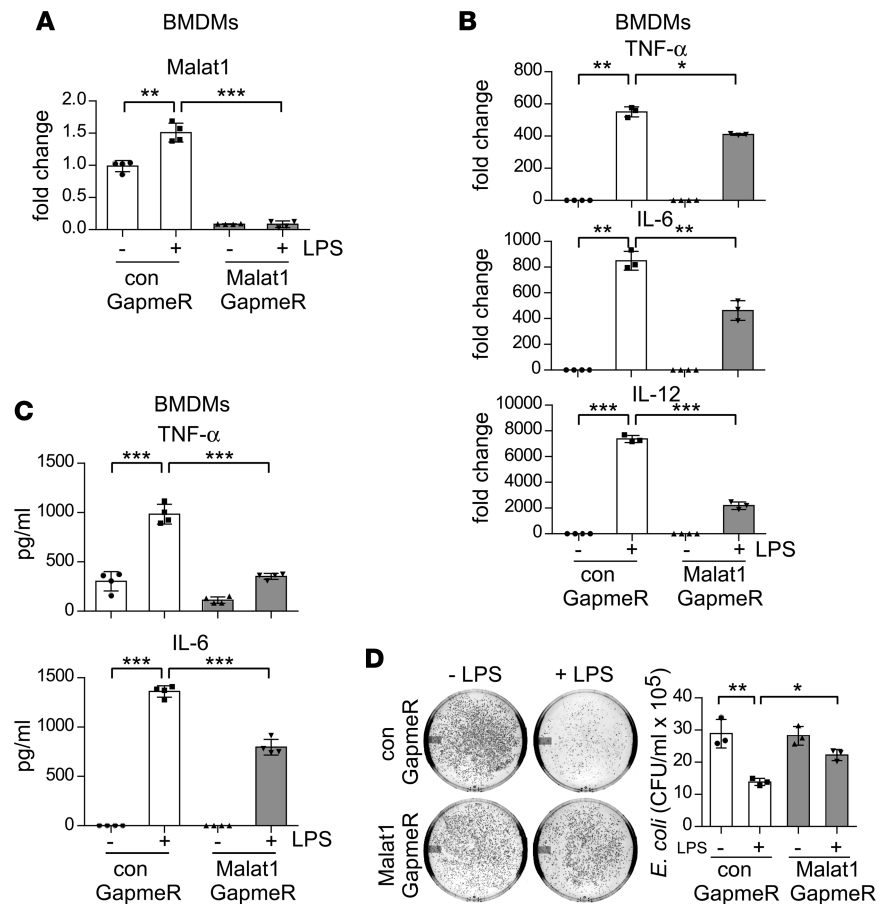
Figure 2. Malat1 knockdown attenuates proinflammatory activation of macrophages. (A) BMDMs were transfected with 20 nM control (con) GapmeR or Malat1 GapmeR. Forty-eight hours after transfection, the cells were treated with or without 100 ng/ml LPS for 6 hours. Total RNAs were isolated and levels of Malat1 determined by real-time PCR. $n = 4$; mean ± SD. (**B** and **C**) Experiments were performed as in **A**. mRNA (**B**) and protein (**C**) levels of the indicated proinflammatory cytokines were determined by real-time PCR or ELISA. $n = 3–4$; mean ± SD. (**D**) Experiments were performed as in **A**. Bacterial killing assay was performed as described in Methods. $n = 3$; mean ± SD. *$P < 0.05$; **$P < 0.01$; ***$P < 0.001$ by 1-way ANOVA with Bonferroni's post hoc test (**A–D**). Representative of more than 3 independent experiments.

autoimmune disease (21–25), which are often associated with aberrant inflammation. We reasoned that Clec16a, like Malat1, may participate in proinflammatory responses. We first confirmed that Clec16a expression was inhibited in Malat1-knockdown macrophages (Figure 3A). We also found that Clec16a was induced by LPS, in a pattern similar to that of the elevation of Malat1 in the treated cells (Figure 3, B–D). To investigate its inflammation-regulatory role, we knocked down Clec16a in macrophages before LPS stimulation. As shown in Figure 3, E and F, Clec16a knockdown attenuated LPS-induced TNF-α, IL-6, and IL-12 at both mRNA and protein levels. To demonstrate if the proinflammatory effect of Malat1 is dependent on Clec16a, we silenced Malat1, Clec16a, or both and found that while the impaired LPS induction of TNF-α and IL-6 by Malat1 knockdown was not completely abrogated, it was clearly attenuated by pre-silencing Clec16a (Figure 3G). Taken together, these data suggest that Clec16a may be a Malat1 mediator playing a critical role in inflammatory responses in macrophages.

Global knockout of Malat1 attenuates endotoxemia-associated systemic and pulmonary inflammation. We had shown that Malat1 was required for the LPS-induced proinflammatory response in macrophages in vitro. We then asked if Malat1 has similar activity in vivo. To answer this question, we utilized the mouse endotoxemia model established by intraperitoneal administration of LPS. We compared the systemic and pulmonary inflammation in global-Malat1-knockout mice (*Malat1*−/−) and wild-type control animals (Supplemental Figure 2). *Malat1*−/− mice revealed no overt phenotype. We first observed that weight loss after LPS administration was mitigated in *Malat1*−/− mice, compared with that in the wild-type controls
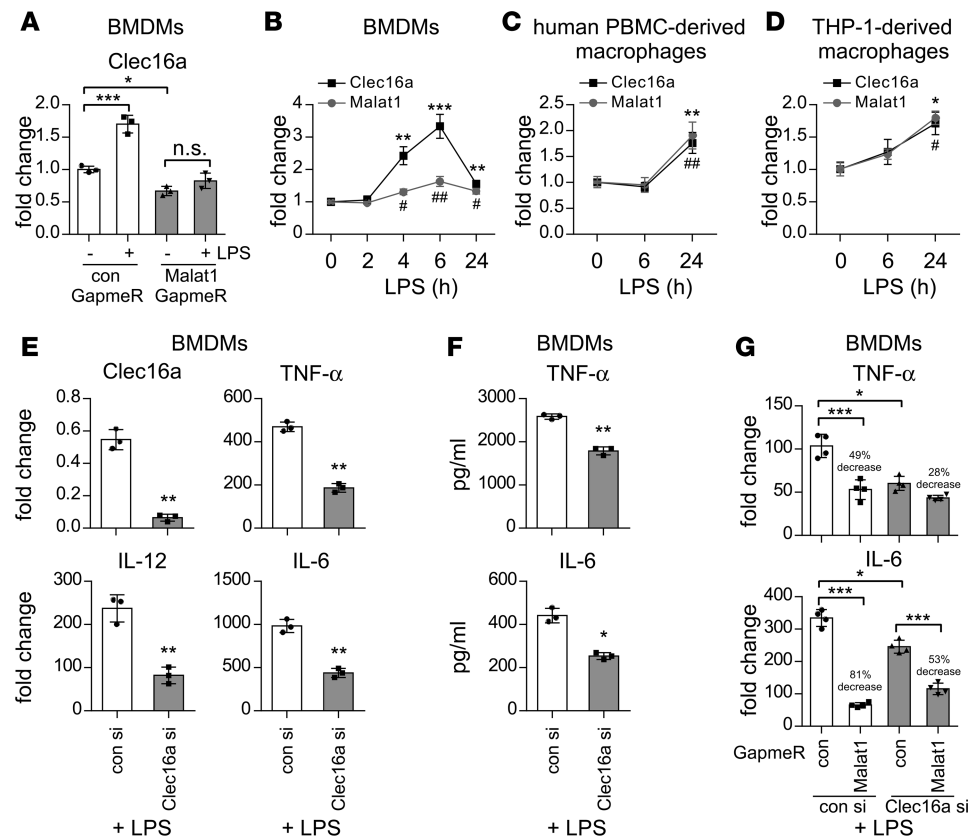
Figure 3. Malat1 regulates the expression of C-type lectin domain family 16, member A (Clec16a), which is required for the proinflammatory activation of macrophages. (**A**) BMDMs were transfected with 20 nM control (con) GapmeR or Malat1 GapmeR. Forty-eight hours after transfection, the cells were treated with or without 100 ng/ml LPS for 6 hours. Total RNAs were isolated and levels of Clec16a determined by real-time PCR. $n = 3$; mean ± SD; *$P < 0.05$, ***$P < 0.001$, one-way ANOVA with Bonferroni's test. (**B–D**) BMDMs (**B**), human PBMC-derived macrophages (**C**), and THP-1–derived macrophages (**D**) were treated with 100 ng/ml LPS for the indicated duration of time. Levels of Clec16a and Malat1 were determined by real-time PCR. $n = 3–4$; mean ± SD; *$P < 0.05$, **$P < 0.01$, ***$P < 0.001$, #$P < 0.05$, ##$P < 0.01$ compared with respective levels at time "0", 2-tailed Student's t test. (**E** and **F**) BMDMs were transfected with 20 nM con siRNA (open bar) or Clec16a siRNA (closed bar). Forty-eight hours after transfection, the cells were treated with or without 100 ng/ml LPS for 6 hours. mRNA (**E**) or protein (**F**) levels of the indicated genes were determined by real-time PCR or ELISA. $n = 3$; mean ± SD; *$P < 0.05$, **$P < 0.01$ compared with the "con si" group, 2-tailed Student's t test. (**G**) BMDMs were cotransfected with con siRNA, con GapmeR, Clec16a siRNA, and Malat1 GapmeR, in combination as indicated. Forty-eight hours after transfection, the cells were treated with or without 100 ng/ml LPS for 6 hours. Levels of the indicated genes were determined by real-time PCR. $n = 4$; mean ± SD; *$P < 0.05$, ***$P < 0.001$, one-way ANOVA with Bonferroni's test. Representative of 2 independent experiments.

(Supplemental Figure 2B), indicating an improved condition in the knockout animals. This notion was further reinforced by the finding that levels of proinflammatory mediators in the sera and lungs of the LPS-treated *Malat1*^{−/−} mice were reduced, compared with those from the LPS-treated wild-type animals (Supplemental Figure 2, C–E). Taken together, these data suggest that Malat1 is proinflammatory in vivo.

Myeloid ablation of Malat1 attenuates LPS-induced acute lung injury. The diminished inflammation in *Malat1*^{−/−} mice with endotoxemia led us to reason that cells of the myeloid lineage, including monocytes, macrophages, and granulocytes, are primary targets of the Malat1 action in this pathology. To test this hypothesis and further define the immune-regulatory role of Malat1 in vivo, we established a strain with conditional knockout of Malat1 in myeloid lineage cells (*Malat1* mye^{−/−}) by crossbreeding *Malat1*^{fl/fl} mice with Lyz2 Cre/Cre animals (Figure 4A). We then administered LPS intratracheally (i.t.) and assessed acute lung injury (ALI) in these mice, as severity of ALI and pulmonary inflammation are known to be well correlated with the immune response of myeloid cells (26). As shown in Figure 4, B–F, we found that levels of pulmonary and bronchoalveolar lavage fluid (BALF) proinflammatory cytokines were significantly decreased in the *Malat1* mye^{−/−} mice, compared with those in the control *Malat1*^{fl/fl} animals. Consistently, LPS-induced

neutrophil infiltration was also diminished in the mice with myeloid ablation of *Malat1* (Figure 4G). The mitigated pulmonary inflammation and injury in the *Malat1* mye$^{-/-}$ mice were further confirmed by histological examination, revealing reduced interstitial thickening, deposition of hyaline membrane, and alveolar accumulation of neutrophils in the lungs of these LPS-treated animals (Figure 4H). To directly determine the effect of Malat1 on cell activation in the inflamed lung, we isolated alveolar macrophages and found that the elevated expression of proinflammatory cytokines was diminished in the cells from the LPS-treated *Malat1* mye$^{-/-}$ animals, compared with that in the *Malat1*$^{fl/fl}$ controls (Figure 4I). Consistently, levels of Clec16a in the alveolar macrophages from *Malat1* mye$^{-/-}$ mice were also decreased, compared with those from the *Malat1*$^{fl/fl}$ animals (Figure 4J). Of note, myeloid ablation of *Malat1* had no effect on the expression of markers and mediators of alternative activation in the alveolar macrophages of the LPS-treated mice (Supplemental Figure 3). Altogether, these data suggest that the weakened proinflammatory response in *Malat1*$^{-/-}$ macrophages, which was presumably mediated by Clec16a downregulation, contributes to the mitigation of LPS-induced ALI in *Malat1* mye$^{-/-}$ animals.

Malat1 knockdown promotes alternative activation of macrophages. It had been previously recognized that certain proinflammatory regulators participate in antiinflammatory M2 activation of macrophages (10). Our finding that IL-4 downregulated Malat1 also alluded to this possibility with this lncRNA. To determine if Malat1 has such an activity, we treated macrophages with IL-4 and found that Malat1 knockdown boosted IL-4–induced M2 polarization, as evidenced by increased expression of M2 phenotypic markers arginase 1 (Arg-1), YM-1, and mannose receptor C-type 1 (MRC1) in these cells, compared with that in IL-4–treated controls (Figure 5, A and B). Similar to the Malat1 effect on M2 activation in vitro, alveolar macrophages from *Malat1*$^{-/-}$ mice that were treated with long-acting IL-4 complex (IL-4c) demonstrated greater expression of Arg-1 and FIZZ1 than those from wild-type animals (Figure 5C). To further define the pro-M2 effect of Malat1 knockdown in macrophages, we examined the real-time oxygen consumption rate (OCR), an indicator of mitochondrial oxidative phosphorylation (OxPhos) in the cells using a Seahorse Analyzer, as it is well known that augmentation of mitochondrial OxPhos is essential to M2 macrophage polarization (27, 28). As shown in Figure 5D, despite the observation that Malat1 knockdown hardly had any effect on OCR in untreated cells, it boosted OCR in IL-4–treated macrophages, consistent with the more pronounced M2 phenotype demonstrated by the same group of cells. Altogether, these data suggest that, in contrast to being proinflammatory, Malat1 is a negative regulator of M2 macrophage polarization.

Next, we examined if the Malat1-regulated proinflammatory Clec16a also participates in M2 macrophage differentiation. Perplexingly, we found that Clec16a knockdown had no effect on IL-4–induced M2 activation (data not shown), suggesting that although Malat1 regulates both M1 and M2 macrophage polarization, it does so via distinct mechanisms. In addition, we found that, similar to the lack of influence on the cytoplasmic events in LPS-treated cells, Malat1 knockdown did not affect IL-4–induced proximal signaling, such as STAT6 phosphorylation and nuclear translocation, in macrophages (Supplemental Figure 1, C and D).

Malat1 regulation of alternative activation of macrophages is dependent on glucose metabolism. Previous studies from our laboratory and others showed that the elevated mitochondrial OxPhos in M2 macrophages was attributable to enhanced glucose metabolism (29, 30). Glucose metabolism consists primarily of two stages, i.e., the cytoplasmic conversion of glucose to pyruvate via glycolysis and the mitochondrial entry of pyruvate to fuel the tricarboxylic acid (TCA) cycle and the ensuing OxPhos for ATP production (30). Given that Malat1 knockdown augmented OCR in IL-4–induced M2 macrophages, we determined if glucose metabolism is involved in the anti-M2 activity of Malat1 in macrophages. We blocked glucose metabolism with 2-deoxy-D-glucose (2-DG), a widely used inhibitor of hexokinases that are the first rate-limiting enzymes of glycolysis (29). As expected, 2-DG diminished the levels of IL-4–induced M2 phenotypic markers (Figure 6A). More importantly, 2-DG abolished the augmented expression of these M2 markers in macrophages with Malat1 knockdown (Figure 6A).

The findings that Malat1 knockdown enhanced OCR in IL-4–induced M2 macrophages and that 2-DG abolished the M2 promotional effect of silencing this lncRNA prompted us to reason that glucose-derived mitochondrial OxPhos is required for the Malat1 regulation of M2 activation. Glucose-derived OxPhos starts with mitochondrial transportation of the glycolytic end-product pyruvate, a process mediated by mitochondrial pyruvate carriers (MPCs) (29, 31). Interestingly, we found that both MPC1 and MPC2 were upregulated by IL-4 (Figure 6B), consistent with previous reports of elevated OxPhos in M2 macrophages (29). More importantly, we found that Malat1 knockdown further enhanced the expression of
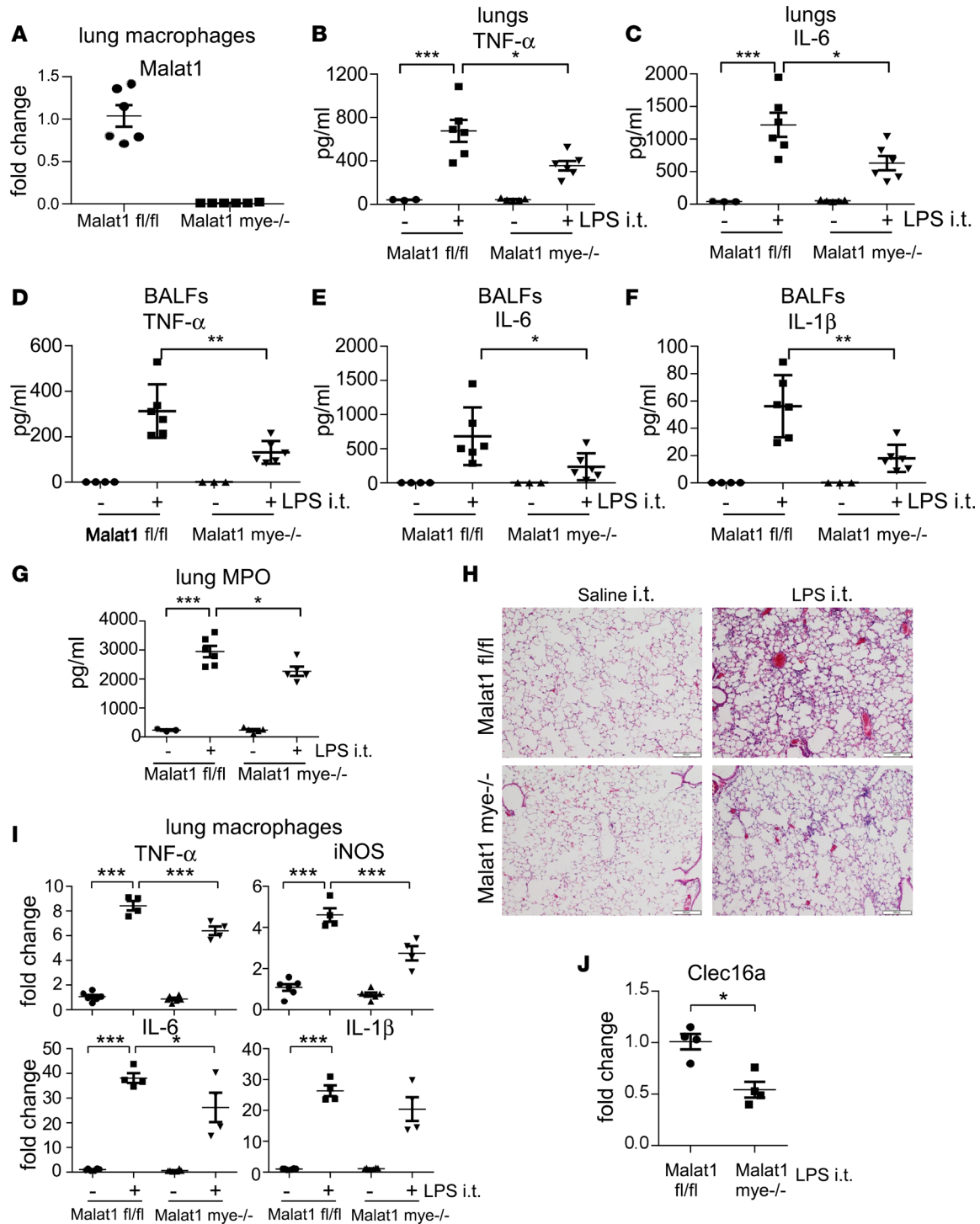
Figure 4. Myeloid ablation of Malat1 (*Malat1* mye⁻/⁻) attenuates LPS-induced ALI. (**A**) Alveolar macrophages were harvested from BALFs of *Malat1^fl/fl^* and *Malat1* mye⁻/⁻ mice. Levels of Malat1 in the cells were determined by real-time PCR. *n* = 6 each for *Malat1^fl/fl^* and *Malat1* mye⁻/⁻ mice; mean ± SE. (**B** and **C**) *Malat1^fl/fl^* and *Malat1* mye⁻/⁻ mice were i.t. instilled with 50 μl saline or 5 mg/kg LPS in 50 μl saline. Forty-eight hours after administration, mice were sacrificed and lung homogenates prepared. Levels of the indicated proinflammatory cytokines were determined by ELISA. *n* = 3, 6, 5, 6 mice for each group; mean ± SE. (**D**–**F**) Experiments were performed as in **B** and **C**. BALF levels of the indicated proinflammatory cytokines were determined by ELISA. *n* = 4, 6, 3, 6 mice for each group; mean ± SE. (**G**) Experiments were performed as in **B** and **C**. Levels of lung MPO were determined by ELISA. *n* = 3, 6, 5, 5 mice for each group; mean ± SE. (**H**) Experiments were performed as in **B** and **C**. H&E staining was performed. Original magnification, ×10. Scale bars: 200 μm. (**I**) Experiments were performed as in **B** and **C**. Twenty-four hours after administration, alveolar macrophages were harvested and mRNA levels of the indicated genes determined by real-time PCR. ● *Malat1^fl/fl^* saline, ■ *Malat1^fl/fl^* LPS, ▲ *Malat1* mye⁻/⁻ saline, ▼ *Malat1* mye⁻/⁻ LPS; *n* = 6, 4, 6, 4 mice for each group; mean ± SE. (**J**) Experiments were performed as in **B** and **C**. Twenty-four hours after administration, alveolar macrophages were harvested and mRNA levels of Clec16a determined. *n* = 4, 4 mice for each group; mean ± SE. *P < 0.05; **P < 0.01; ***P < 0.001 by 1-way ANOVA with Bonferroni's post hoc test (**B**–**I**) or 2-tailed Student's *t* test (**J**).
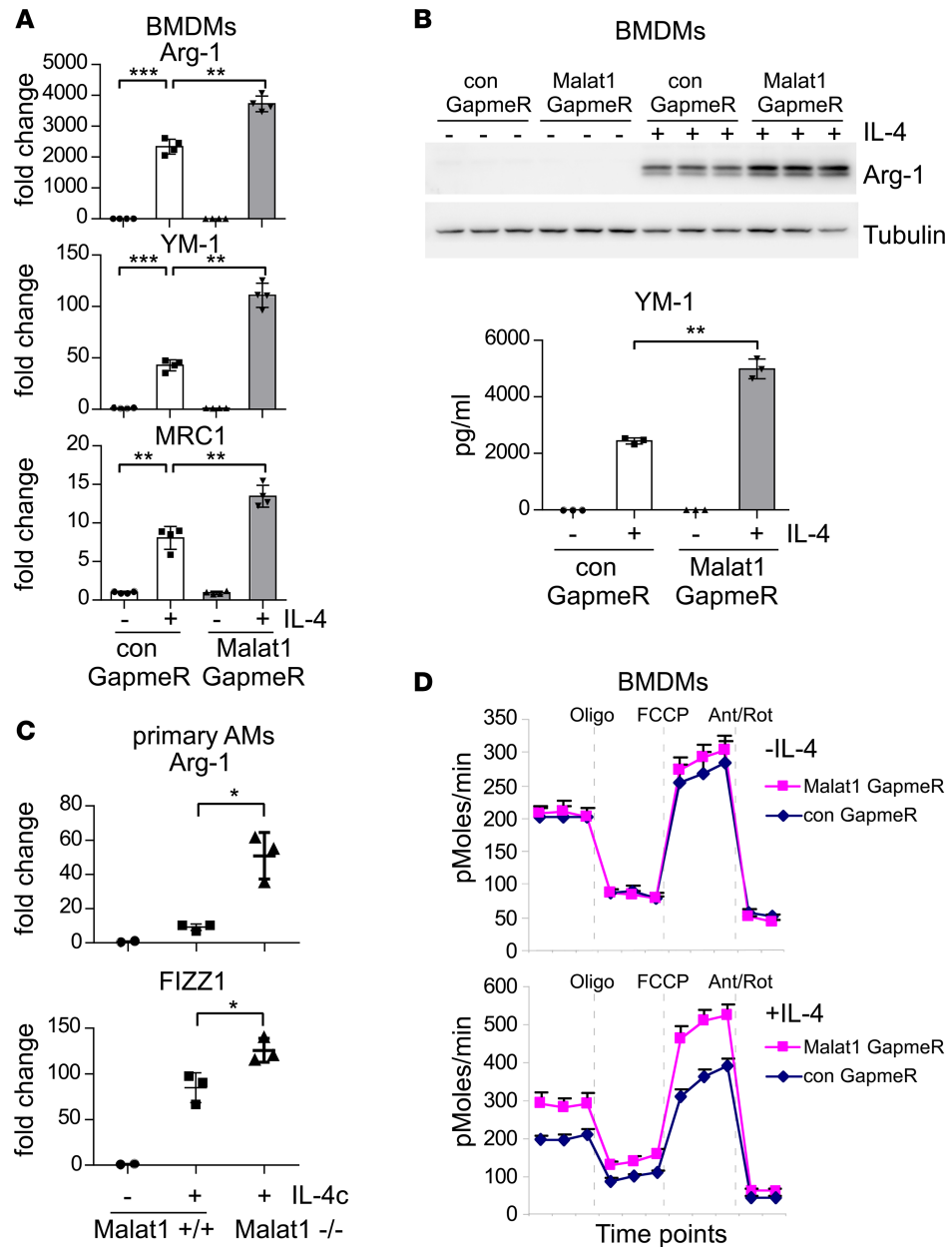
Figure 5. Malat1 knockdown promotes alternative activation of macrophages. (A) BMDMs were transfected with 20 nM control (con) GapmeR or Malat1 GapmeR. Forty-eight hours after transfection, the cells were treated with or without 5 ng/ml IL-4 for 24 hours. Levels of the indicated genes were determined by real-time PCR. $n = 4$; mean ± SD. **(B)** Experiments were performed as in **A**. Levels of Arg-1 and YM-1 were determined by Western blotting or ELISA. $n = 3$; mean ± SD. **(C)** $Malat1^{fl/fl}$ and $Malat1$ mye$^{-/-}$ mice were i.t. instilled with IL-4 (1 μg)/anti–IL-4 antibody (5 μg) immunocomplex (IL-4c) in 50 μl saline. Twenty-four hours after administration, alveolar macrophages were harvested and levels of the indicated genes determined. $n = 2, 3, 3$ mice for each group; mean ± SE. **(D)** BMDMs were transfected with 20 nM con GapmeR or Malat1 GapmeR. Twenty-four hours after transfection, the cells were trypsinized and plated on Seahorse XF-24 microplates. Twenty-four hours after plating, the cells were treated without (top) or with (bottom) 5 ng/ml IL-4 for 24 hours. The media were then replaced with OCR assay media and cultured for 1 hour, followed by sequential treatments with 3 μg/ml oligomycin (Oligo), 6 μM FCCP, and 1 μM rotenone (Rot) plus 0.5 μM antimycin A (Ant). Real-time OCR was recorded. $n = 5$ for each condition; mean ± SE. Representative of 2 to 4 independent experiments. $*P < 0.05$; $**P < 0.01$; $***P < 0.001$ by 1-way ANOVA with Bonferroni's post hoc test.

MPC1 and MPC2 (Figure 6B). Together with the finding that Malat1 knockdown augmented OCR in M2 macrophages, these data suggest that Malat1 regulates glucose-derived mitochondrial OxPhos through controlling MPC-mediated mitochondrial entry of pyruvate. To further test this hypothesis, we blocked pyruvate mitochondrial entry in macrophages with UK-5099, a well-defined inhibitor of MPCs (29, 31),
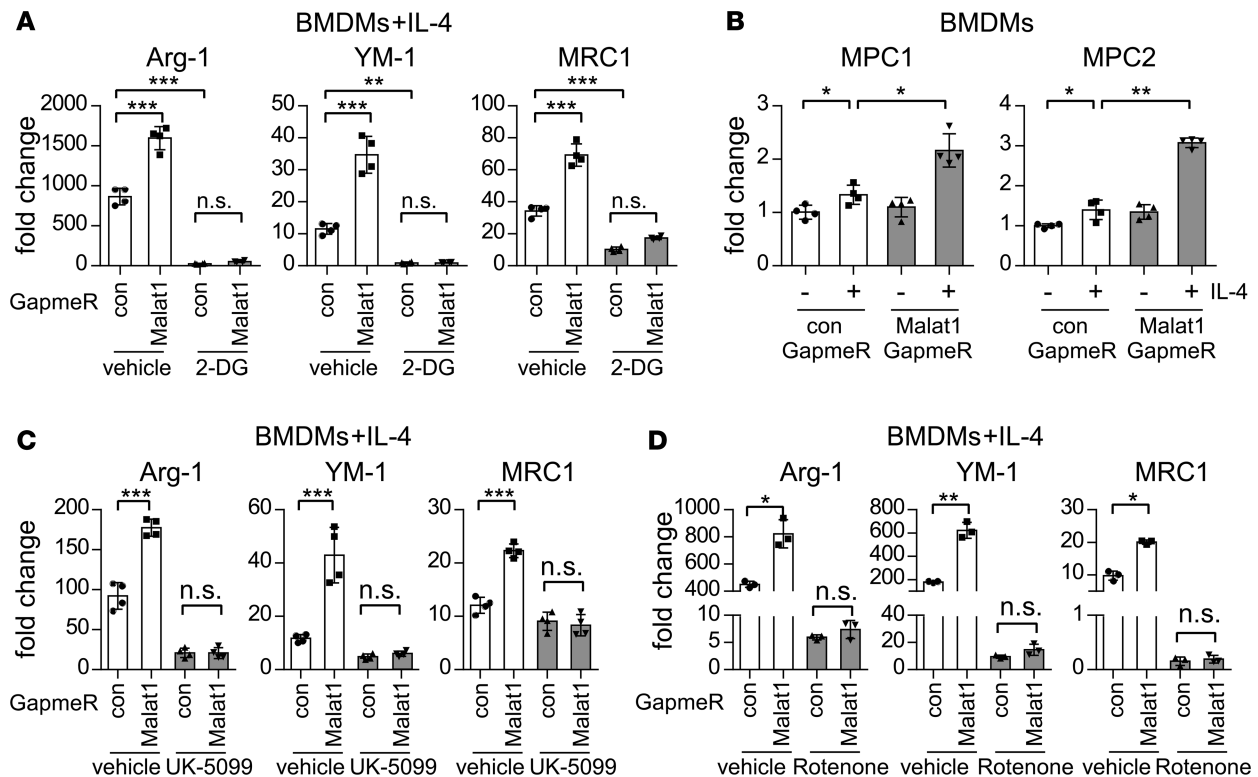
Figure 6. Malat1 regulation of alternative activation of macrophages is dependent on glucose metabolism. (**A**) BMDMs were transfected with 20 nM control (con) GapmeR or Malat1 GapmeR. Forty-eight hours after transfection, the cells were pretreated with vehicle or 2 mM 2-DG for 1 hour, followed by treatment with 5 ng/ml IL-4 for 12 hours. Levels of the indicated M2 markers were determined by real-time PCR. $n = 4$; mean ± SD. (**B**) BMDMs were transfected with 20 nM con GapmeR or Malat1 GapmeR. Forty-eight hours after transfection, the cells were treated with or without 5 ng/ml IL-4 for 12 hours. Levels of MPC1 and MPC2 were determined by real-time PCR. $n = 4$; mean ± SD. (**C** and **D**) The experiments were performed as in **A**, except that the cells were pretreated with vehicle, 50 μM UK-5099 (**C**), or 200 nM rotenone (**D**) for 1 hour. $n = 3$–4; mean ± SD. $*P < 0.05$; $**P < 0.01$; $***P < 0.001$ by 1-way ANOVA with Bonferroni's post hoc test (**A**–**D**). Representative of 2 to 4 independent experiments.

and found that UK-5099 inhibited the expression of the IL-4–induced M2 markers (Figure 6C). Moreover, inhibition of pyruvate mitochondrial entry eliminated the enhanced M2 phenotype in macrophages with Malat1 knockdown (Figure 6C). Together, these data indicate a dependence on the glucose-derived mitochondrial OxPhos of the M2-regulatory role of Malat1. This notion was reinforced by the finding that direct inhibition of OxPhos by the complex-I inhibitor rotenone also abrogated the augmented M2 activation in Malat1-knockdown macrophages (Figure 6D). These data, together with the finding of IL-4 downregulation of Malat1, suggest that Malat1 and Malat1-regulated glucose-derived mitochondrial OxPhos constitute a positive feedback loop to control M2 macrophage polarization.

Malat1 knockdown promotes profibrotic differentiation of macrophages. We had shown the Malat1 inhibition of IL-4–induced M2 activation in vitro and in vivo. In addition, we had found that the Malat1 regulation of alternative activation of macrophages required glucose metabolism. Because there had been wide recognition that a subtype of alternatively activated macrophages play a critical role in wound healing, tissue remodeling, and organ fibrosis (1, 2), and we previously found that the profibrotic phenotype of lung macrophages from mice with experimental pulmonary fibrosis was dependent on glycolysis, we were intrigued to ask if Malat1 would regulate the macrophage profibrotic phenotype in the context of lung fibrosis. Our hypothesis was that profibrotic stimuli downregulated macrophage Malat1 to promote pathological fibrogenesis.

Macrophages in mouse pulmonary alveoli are exclusively resident alveolar macrophages. However, alveolar macrophages in mice with bleomycin-induced pulmonary fibrosis are a heterogeneous population consisting of resident alveolar macrophages and those infiltrating from the pulmonary interstitium (also often termed recruited alveolar macrophages). We purified resident alveolar macrophages and the recruited ones by FACS and found that the Malat1 level was decreased in the resident alveolar macrophages from bleomycin-treated mice (Figure 7A). In addition, the Malat1 level in recruited macrophages was even lower than that of the resident alveolar macrophages from fibrotic lungs (Figure 7A).
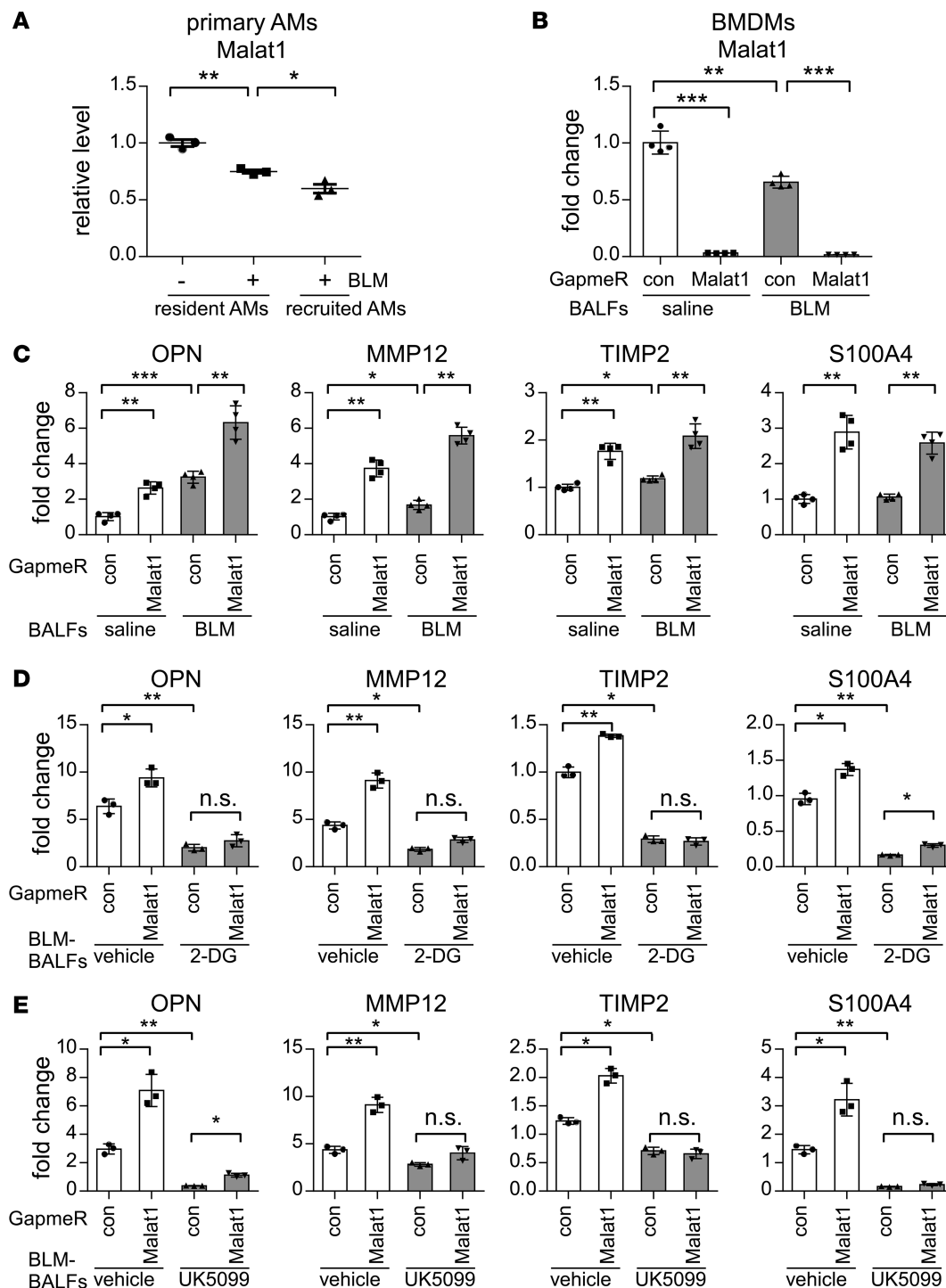
Figure 7. Malat1 knockdown promotes profibrotic differentiation of macrophages. (**A**) Wide-type mice were i.t. instilled with 50 μl saline or 1.5 U/kg bleomycin (BLM) in 50 μl saline. Three weeks after bleomycin administration, BAL cells were collected and resident and recruited alveolar macrophages were sorted as described in Methods. Levels of Malat1 were determined by real-time PCR. *n* = 3, 3 mice for each group; mean ± SE. (**B** and **C**) BMDMs were transfected with 20 nM control (con) GapmeR or Malat1 GapmeR. Forty-eight hours after transfection, the cells were treated for 48 hours with BALFs from mice that were treated i.t. with saline or 1.5 U/kg bleomycin for 3 weeks. Levels of the indicated genes were determined by real-time PCR. *n* = 4; mean ± SD. (**D** and **E**) BMDMs were transfected with 20 nM con GapmeR or Malat1 GapmeR. Forty-eight hours after transfection, the cells were pretreated with vehicle, 2 mM 2-DG (**D**), or 50 μM UK-5099 (**E**) for 1 hour, followed by treatment with BALFs from mice that were treated i.t. with saline or 1.5 U/kg bleomycin for 3 weeks. Levels of the indicated profibrotic markers were determined by real-time PCR and normalized to the group of cells treated with con GapmeR and saline BALF. *n* = 3; mean ± SD. *P < 0.05; **P < 0.01; ***P < 0.001 by 1-way ANOVA with Bonferroni's post hoc test (**A**–**E**). Representative of 2 independent experiments.

We also treated macrophages with BALFs from control mice or mice with bleomycin-induced pulmonary fibrosis to establish an ex vivo pathogenic setting because BALFs from fibrotic mouse and human lungs contain a number of profibrotic mediators, such as TGF-β1 and osteopontin (OPN). We found that BALFs from fibrotic lungs inhibited macrophage Malat1 expression (Figure 7B), consistent with the reduced expression of this lncRNA in the alveolar macrophages from fibrotic lungs. Furthermore, knockdown of Malat1 promoted the expression of a selected array of profibrotic mediators, including OPN, MMP12, TIMP2, and S100A4 (32), in macrophages incubated with BALFs from saline- and bleomycin-treated mice (Figure 7C), indicating Malat1 participation in pathological fibrogenesis through controlling the profibrotic phenotype of macrophages in the lung. To determine the role of glucose metabolism in Malat1 regulation of the profibrotic phenotype, we used 2-DG to block this metabolic pathway and found that 2-DG eliminated the augmented expression of these profibrotic markers in the macrophages with Malat1 knockdown (Figure 7D). We also treated macrophages with the MPC inhibitor UK-5099 and found that it inhibited the expression of profibrotic markers induced by BALFs from mice with lung fibrosis. More importantly, UK-5099 almost completely abolished the enhanced profibrotic phenotype in the cells with Malat1 knockdown (Figure 7E). Together, these data suggest a dependence of Malat1 regulation of the macrophage profibrotic phenotype on glucose-derived mitochondrial OxPhos.

Myeloid ablation of Malat1 promotes bleomycin-induced pulmonary fibrosis. We had shown that Malat1 inhibited the profibrotic macrophage phenotype induced by BALFs from lungs of bleomycin-treated mice in vitro. We also found that the expression of alveolar macrophage Malat1 was decreased in fibrotic mouse lungs. This body of evidence suggests that macrophage Malat1 may have an important role in developing this pathology. To test the hypothesis, we again resorted to the mouse model of bleomycin-induced pulmonary fibrosis, as lung macrophages are known to be essential to the pathogenesis of this disease (33, 34). Indeed, we found that bleomycin-induced pulmonary collagen deposition, as reflected by the level of hydroxyproline, was significantly increased in mice with ablation of macrophage Malat1, compared with that in the control animals (Figure 8A). These data suggest that macrophage Malat1 is protective from developing pulmonary fibrosis. Additionally, Masson's trichrome staining of lung collagen, histological examination of the lungs, and immunohistochemical analyses of α smooth muscle actin (α-SMA) and fibronectin all confirmed the increased severity in bleomycin-induced pulmonary fibrosis in macrophage-Malat1-ablated mice (Figure 8B and Supplemental Figure 4).

To determine the role of the Malat1-regulated lung macrophage phenotype in pulmonary fibrosis, we first ruled out the possibility that the elevated lung fibrosis in macrophage-Malat1-ablated mice was simply caused by an abnormal macrophage infiltration because we found that there was no difference in total numbers of alveolar macrophages or the ratios of resident to recruited alveolar macrophages between the bleomycin-treated wild-type and knockout animals (Figure 8, C and D). We then compared the expression of differential activation markers and mediators in the alveolar macrophages from bleomycin-treated *Malat1* mye$^{-/-}$ and the control *Malat1*$^{fl/fl}$ mice. As shown in Figure 8, E and F, there was elevated expression of Arg-1, MSR1, PPARγ, and KLF4 in alveolar macrophages from bleomycin-treated control mice. More importantly, we found that the elevation in these molecules was further augmented in alveolar macrophages from bleomycin-treated mice with Malat1 ablation in these cells (Figure 8E). Of note, Malat1 ablation had no effect on expression of M1 phenotypic markers in macrophages from fibrotic lungs (Figure 8F). Because a characteristic of lung macrophages in fibrotic lungs is their effusive production of profibrotic mediators, such as OPN, S100A4, PDGF-α, MMPs, and TIMP2 (32), we investigated if Malat1 regulates the profibrotic phenotype of these cells. Similarly to the alternative markers, the production of the profibrotic mediators was also further enhanced in alveolar macrophages from bleomycin-treated *Malat1* mye$^{-/-}$ mice (Figure 8G). Consistent with the upregulated expression of MPC1 and MPC2 in Malat1-knockdown M2 macrophages in vitro, the levels of these 2 proteins were augmented in alveolar macrophages from the fibrotic lungs of *Malat1* mye$^{-/-}$ mice (Figure 8H). Altogether, these data suggest that the Malat1 regulation of M2 and profibrotic phenotypes in lung macrophages plays an important role in the pathogenesis of pulmonary fibrosis.

Discussion

The regulation of macrophage activation has been under extensive investigation, particularly at transcriptional and epigenetic levels (1). In the past decade, it has been increasingly clear that small ncRNAs, e.g., miRs, also play a crucial role in this process (11). A number of miRs have since been found to be intrinsically involved in a variety of pathogeneses through regulating macrophage activation (11).
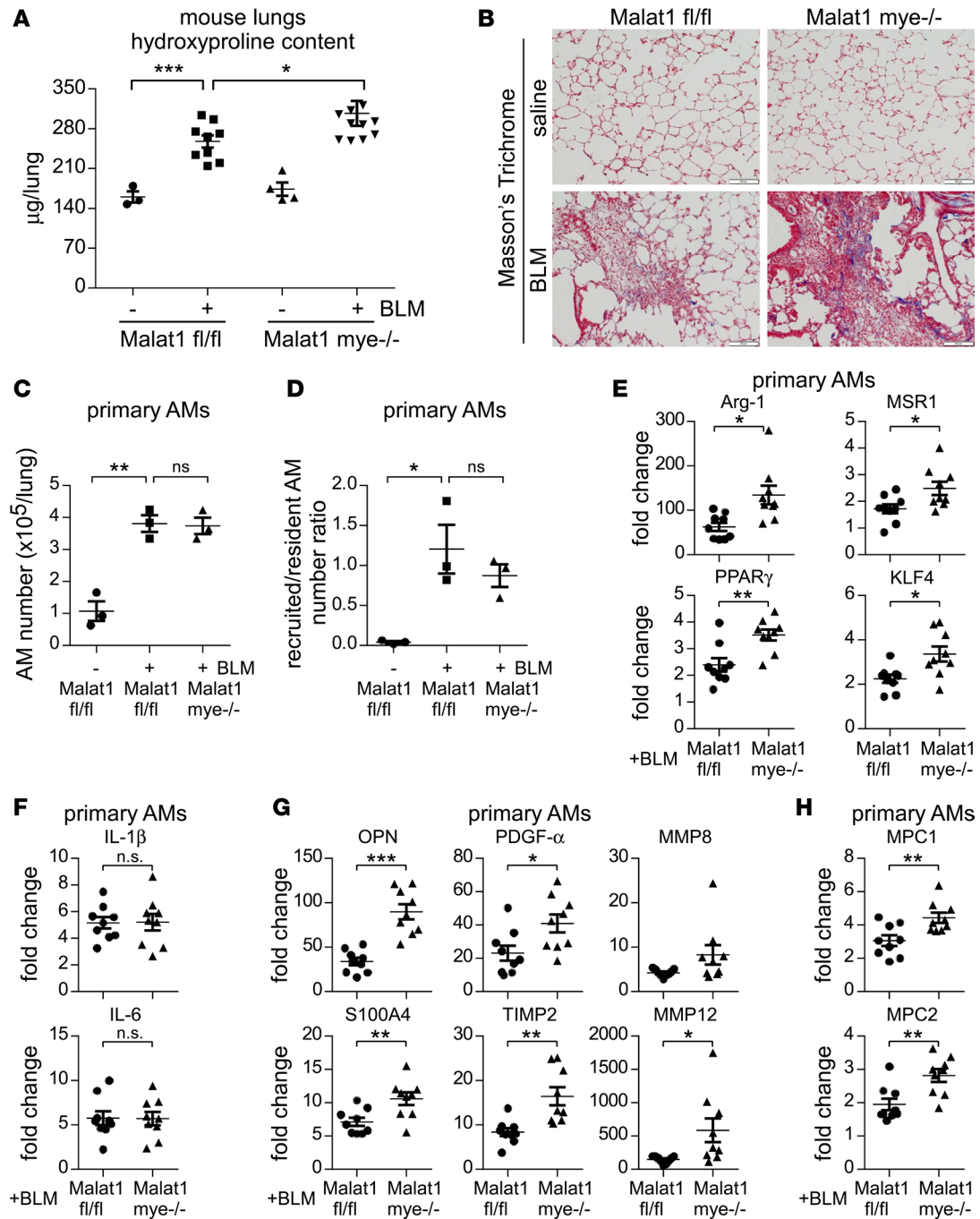
Figure 8. Myeloid ablation of Malat1 promotes bleomycin-induced pulmonary fibrosis. (**A**) *Malat1*^{fl/fl} and *Malat1* mye^{−/−} mice were i.t. instilled with 50 μl saline or 1.5 U/kg bleomycin (BLM) in 50 μl saline. Three weeks after bleomycin administration, mice were sacrificed and lung homogenates prepared. Levels of hydroxyproline in the whole lungs were determined. n = 3, 9, 4, 10 mice for each group; mean ± SE. (**B**) The experiments were performed as in **A**. Lungs were fixed with 10% formalin and sections prepared. Masson's trichrome staining was performed. Original magnification, ×20. Scale bars: 100 μm. (**C** and **D**) The experiments were performed as in **A**. BAL cells were collected and resident and recruited macrophages sorted. Total alveolar macrophage numbers (**C**) and relative numbers of resident and recruited macrophages (**D**) were determined. n = 3, 3, 3 mice for each group; mean ± SE. (**E**–**H**) The experiments were performed as in **A**. BALFs were prepared and alveolar macrophages in the BALFs harvested. Levels of the indicated genes in the cells were determined by real-time PCR. ● *Malat1*^{fl/fl} BLM, ▲ *Malat1* mye^{−/−} BLM; n = 9 mice for each group; mean ± SE. $*P < 0.05$; $**P < 0.01$; $***P < 0.001$ by 1-way ANOVA with Bonferroni's post hoc test (**A**, **C**–**H**).

However, although a much greater number of lncRNAs exist in mammalian cells, their role in this process remains poorly understood. In this study, we demonstrate that Malat1 is a key player in controlling macrophage phenotype in that this lncRNA not only promotes proinflammatory M1 activation, it also inhibits the alternative M2 and profibrotic activation. Our study has thus added Malat1 to an emerging

list of lncRNAs that demonstrate an important regulatory role in macrophage polarization (35, 36).

Although Malat1 is upregulated in LPS-treated macrophages and it promotes proinflammatory activation of macrophages in vitro, it is clinically more significant to find that Malat1 participates in the pathogeneses of inflammatory diseases, such as ALI, in the mouse model. Understanding this process provides insight into the molecular mechanism underlying similar human disorders and warrants further studies to associate Malat1 level with disease severity and prognosis of patients. Indeed, there is currently little investigation into this subject, despite the fact that Malat1 upregulation has been frequently implicated in the initiation and progression of many cancers (13, 37). Additionally, our study also identifies a potential therapeutic target in Malat1 for treating aberrant inflammation caused by excessively activated macrophages.

Our RNA-seq analysis reveals that the *Clec16a* transcript has the greatest decline in Malat1-knockdown macrophages. Although the underlying mechanism is currently unknown, there are several possibilities to be considered. First, Malat1 has been shown to directly regulate gene transcription through interactions with transcriptional factors and epigenetic modifiers (37, 38). Additionally, Malat1 also participates in mRNA splicing and thereby controls the relative expression of different gene isoforms (12, 39, 40). These mechanistic processes could also account for the Malat1-dependent Clec16a expression. There are also reports that Malat1 can serve as a sponge for specific miRs in several types of cancer cells and thereby shields miR targets from degradation (41). However, this is unlikely to be the mechanism underlying Malat1's regulatory role in macrophage activation, because miR/mRNA interaction takes place primarily in the cytoplasm, whereas Malat1 is predominantly nuclear in macrophages.

Clec16a was initially identified as a diabetes-associated gene one decade ago (21). However, the molecular function of Clec16a has been unclear, despite recent studies showing that it has an important role in autophagy (42, 43). Although it remains to be seen if autophagy is involved in the proinflammatory activity of Clec16a, it may just function like other C-type lectins after all. Indeed, there has been overwhelming evidence that this group of molecules are important mediators of inflammation in various pathophysiological conditions (44, 45).

We found that Malat1 knockdown enhances the glucose-derived mitochondrial OxPhos, which seems to contribute to the augmented M2 macrophage phenotype in these cells. The Malat1 regulation of glucose-derived mitochondrial OxPhos is apparently dependent on its controlling of the expression of MPCs. However, in contrast to regulating Clec16a at the basal level, Malat1 modulates only the IL-4–induced MPCs (Figure 6B, and data not shown). Although these data are in accordance with the RNA-seq analysis, which does not identify MPCs as potential Malat1 targets at the basal level (Supplemental Table 1), as well as the OCR revelation of no effect of Malat1 knockdown on mitochondrial OxPhos in untreated macrophages (Figure 5D), we have to acknowledge that it remains to be determined how Malat1 can distinctly regulate the expression of various mediators to achieve its differential regulation of macrophage activation. Nevertheless, it is plausible that Malat1 may associate with specific transcriptional factors/coregulators in uniquely temporospatial manners, which are likely dictated by a number of factors, such as the nature of posttranslational modifications on these molecules.

Alternatively activated macrophages are well known to be critical contributors to injury repair and fibrosis, allergic reaction, angiogenesis, and tumor progression (1, 2, 9). Although these cells are historically referred to as M2 macrophages collectively, it is now quite clear that they also demonstrate a great deal of functional diversity, including those displayed in IL-4–dependent type II immunity as well as in the wound healing process (1, 46). We and others previously found that glucose metabolism was augmented not only in the typical IL-4–induced M2 macrophages, but also in profibrotic alveolar macrophages from mice with experimental pulmonary fibrosis (29, 30, 32). We show here that Malat1 knockdown augments both the M2 and profibrotic phenotypes in macrophages. Taken together, this body of evidence suggests that the Malat1 regulation of glucose metabolism is likely a common mechanism that various alternatively activated macrophages rely on to sustain their distinctive phenotype. Malat1 dysregulation has thus become a defining feature shared by these pathologies that involve aberrant alternative and profibrotic activation of macrophages.

We have characterized what we believe is a novel role of Malat1 in controlling macrophage polarization. Our data demonstrate that Malat1 is critically involved in the pathogenesis associated with aberrant macrophage activation and identify Malat1 as a potential therapeutic target for treating this group of disorders.

Methods

Reagents. Ultra-pure LPS from *Escherichia coli* O111:B4, 2-DG, and UK-5099 were from Sigma-Aldrich. Mouse recombinant IL-4 was from PeproTech. InVivoMAb anti–mouse IL-4 was from Bio X Cell.

Mice. Eight-week-old male C57BL/6 mice and myeloid lineage Cre mice Lyz2 Cre/Cre were purchased from The Jackson Laboratory. *Malat1⁻/⁻* and *Malat1ᶠˡ/ᶠˡ* mice were described previously (47). Mice with myeloid ablation of Malat1, *Malat1* mye⁻/⁻, were established by cross-breeding *Malat1ᶠˡ/ᶠˡ* mice with the Lyz2 Cre/Cre line.

Establishment of mouse BMDMs, human PBMC-derived macrophages, and THP-1–derived macrophages. Mouse BMDMs were derived from bone marrow cells of C57BL/6 mice as previously described (48). Briefly, following erythrocyte lysis, bone marrow cells were cultured in DMEM containing 10% FBS and 50 ng/ml murine macrophage colony-stimulating factor (M-CSF) (R&D Systems) for 5 days. The differentiated cells were then split and plated for subsequent experiments. To establish human macrophages, human PBMCs (Zen-Bio) were cultured in DMEM containing 10% FBS and 50 ng/ml human M-CSF for 5 days. Human monocytic THP-1 cells (ATCC) were induced into macrophages by 24 hours of incubation with 100 nM phorbol 12-myristate 13-acetate (PMA) (Sigma-Aldrich), followed by another 3 days of culture in DMEM containing 10% FBS.

Isolation of mouse alveolar macrophages. Mouse alveolar macrophages (AMs) were isolated as previously described with some modifications (32, 49, 50). Briefly, BALFs were harvested and BAL cells were collected by centrifugation. After red blood cell lysis, BAL cells were plated for 1 hour, followed by extensive washing to remove unattached cells. The attached cells were used as AMs. Alternatively, BAL cells were preblocked with mouse Fc Block (BD Biosciences) in PBS containing 1% BSA, followed by staining with a mixture of fluorochrome-conjugated antibodies including PerCP/Cy5.5 anti-CD64 (BioLegend, clone X54-5/7.1), eFluor 450 anti-F4/80 (eBioscience, clone BM8), Alexa Fluor 488 anti-CD11b (eBioscience, clone M1/70), and eFluor 660 anti-CD170 (Siglec F) (eBioscience, clone 1RNM44N). FACS was performed on a FACSAria II instrument (BD Biosciences), and resident (CD64⁺F4/80⁺Siglec FʰⁱCD11bˡᵒ) and recruited alveolar macrophages (CD64⁺F4/80⁺Siglec FˡᵒCD11bʰⁱ) were sorted and collected for further analysis.

Establishment of LPS-induced endotoxemia. Mice were injected intraperitoneally with LPS (10 mg/kg body weight in 50 μl saline). Eighteen hours after injection, mice were weighed and sacrificed. Mouse whole blood was collected via cardiac puncture and sera prepared.

Establishment of LPS-induced ALI. Mice were i.t. instilled with LPS (5 mg/kg body weight in 50 μl saline). Forty-eight hours after i.t. instillation, mice were sacrificed and the following assays were performed to evaluate severity of lung injury: (a) determination of BALF and lung proinflammatory cytokine levels, (b) determination of lung myeloperoxidase (MPO) levels, and (c) lung histological evaluation.

Experimental pulmonary fibrosis model. The bleomycin-induced lung fibrosis mouse model was previously described (51).

Hydroxyproline level determination. The right 3 lobes and the left upper lobe of mouse lungs were homogenized in 3 ml H$_2$O. Homogenates (100 μl) were mixed with 100 μl 12N HCl and the samples incubated at 120°C for 3 hours. Hydroxyproline levels were then determined with BioVision's Hydroxyproline Assay Kit according to the manufacturer's instructions.

Immunohistochemistry and Masson's trichrome staining. Immunohistochemistry for α-SMA and fibronectin and Masson's trichrome staining for collagen deposition were performed as described previously (52). Rabbit anti–α-SMA antibody (catalog 23081-1-AP) was from Proteintech, and mouse anti-fibronectin antibody (catalog F7387) was from Sigma-Aldrich.

siRNA and GapmeR transfection. siRNA and GapmeR transfections were performed using HiPerFect reagents (Qiagen) according to the manufacturer's instructions. ON-TARGETplus negative control siRNA pool and specific mouse Clec16a siRNA pool were from Dharmacon. Control and mouse Malat1 GapmeRs were from Qiagen.

RNA-seq assay. RNA-seq was performed by the University of Alabama at Birmingham Heflin Center for Genomic Science. RNA-seq data were submitted to NCBI's Gene Expression Omnibus and are unrestrictedly accessible with accession number GSE106913 (https://www.ncbi.nlm.nih.gov/geo/query/acc.cgi?acc=GSE106913).

Real-time PCR. mRNA levels were determined by real-time PCR using SYBR Green Master Mix Kit (Roche). Primer sequences for human genes were Malat1 sense, 5′-GGGGGAGTTTTCAGTATTTTTTTTG-3′ and antisense, 5′-TACACCTTGAGTCATTTGCCTTTAGG-3′; tubulin β1 sense, 5′-TGGACTCTGTTCGCTCAGGTCCTT-3′ and antisense, 5′-AGTGGCCTTTGGCCCAGTTGTTAC-3′; Clec16a sense, 5′-GTTCAAAAGGCATCAAGACGAGTGG-3′ and antisense, 5′-AGACATGGCATAGAGGAGGCAGAG-3′. Primer sequences for mouse genes were Malat1 sense, 5′-GGGAGTGGTCTTAACAGGGAGGAG

3′ and antisense, 5′-GTGCCAACAGCATAGCAGTACACG-3′; tubulin α1 sense, 5′-GGATGCTGCCAATA-ACTATGCTCGT-3′ and antisense, 5′-GCCAAAGCTGTGGAAAACCAAGAAG-3′; Arg-1 sense, 5′-TGACT-GAAGTAGACAAGCTGGGGAT-3′ and antisense, 5′-CGACATCAAAGCTCAGGTGAATCGG-3′; YM-1 sense, 5′-ATGAAGCATTGAATGGTCTGAAAG-3′ and antisense, 5′-TGAATATCTGACGGTTCTGAG-GAG-3′; MRC1 sense, 5′-GGGCAGTCACCATATTTTATTGGC-3′ and antisense, 5′-GCAAAGTTGG-GTTCTCCTGTAGCC-3′; MSR1 sense, 5′-TGTCAGAGTCCGTGAATCTACAGCAAA-3′ and antisense, 5′-CAGTGTCTGTGAGTGTTCCCAGTCCTT-3′; PPARγ sense, 5′-TGATCAAGAAGACAGAGACAGA-CA-3′ and antisense, 5′-TAGTGCAATCAATAGAAGGAACACG-3′; KLF4 sense, 5′-TACCCTCCTTTCCT-GCCAGACCA-3′ and antisense, 5′-GCCACGACCTTCTTCCCCTCTTT-3′; TNF-α sense, 5′-AAATTC-GAGTGACAAGCCTGTAGCC-3′ and antisense, 5′-GTTGGTTGTCTTTGAGATCCATGCC-3′; IL-6 sense, 5′-CCCAATTTCCAATGCTCTCCTA-3′ and antisense, 5′-AGGAATGTCCACAAACTGTATAT-GCT-3′; IL-12p40 sense, 5′-CCAAATTACTCCGGACGGTTCAC-3′ and antisense, 5′-CAGACAGAGAC-GCCATTCCACAT-3′; IL-1β sense, 5′-AAGGAGAACCAAGCAACGACAAAATA-3′ and antisense, 5′-TTTCCATCTTCTTCTTTGGGTATTGC-3′; Clec16a sense, 5′-AGGAGGAGGACGAGGAGAGAG-GGT-3′ and antisense, 5′-GCATACAGGAGGCAGAGCACGAAG-3′; MPC1 sense, 5′-TCGCCCTCT-GTTGCTATTCTCTGAC-3′ and antisense, 5′-TTCAAGAGCTGGTCCTTGTACCGC-3′; MPC2 sense, 5′-AATTGAGGCCGCTTTACAACCACC-3′ and antisense, 5′-CCAGCACACACCAATCCCCATTTC-3′; OPN sense, 5′-GCCGAGGTGATAGCTTGGCTTATG-3′ and antisense, 5′-CTCTCCTGGCTCTCTTTG-GAATGC-3′; S100A4 sense, 5′-TCCACAAATACTCAGGCAAAGAGGG-3′ and antisense, 5′-TGTTGCT-GTCCAAGTTGCTCATCAC-3′; PDGF-α sense, 5′-CTGTTGTAACACCAGCAGCGTCAAGT-3′ and antisense, 5′-CATTGGCAATGAAGCACCATACATAG-3′; TIMP2 sense, 5′-GCAACCCCATCAAGAG-GATTCAGT-3′ and antisense, 5′-CTTCTGGGTGATGCTAAGCGTGTC-3′; MMP8 sense, 5′-GGTTAC-CCCAAAAGCATACCAAGC-3′ and antisense, 5′-CTCTGTGACTGACAAAATTAAATGCAAAA-3′; MMP12 sense, 5′-CACTTCCCAGGAATCAAGCCTAAAAT-3′ and antisense, 5′-AAAACCAGCAAG-CACCCTTCACTACA-3′. To calculate fold change in the expression of these genes, ΔCt = Ct of tubulin – Ct of individual genes was first obtained. ΔΔCt = ΔCt of treated groups – ΔCt of untreated control groups was then obtained. Fold change was calculated as $2^{\Delta\Delta Ct}$, with control groups set to 1-fold.

Western blotting. Western blotting was performed as previously described (53). Mouse anti–α-tubulin antibody (catalog T5168) was from Sigma-Aldrich. Goat anti–lamin B1 (catalog sc-6216) and rabbit anti-Arg-1 (catalog sc-20150) antibodies were from Santa Cruz Biotechnology. Rabbit anti-p65 (catalog 8242S), –p-p65 (catalog 3033S), –p-IκB-α (catalog 9246S), -STAT6 (catalog 9362S), –p-STAT6 (catalog 9361S), -iNOS (catalog 13120S), and -GAPDH (catalog 5174S) antibodies were from Cell Signaling Technology. Goat anti–mIL-1β antibody (catalog AF-401-NA) was from R&D Systems. See complete unedited blots in the supplemental material.

ELISA. Levels of TNF-α, IL-6, YM-1, and MPO in cell culture supernatants, BALFs, Sera, or lung tissue extracts were determined using DuoSet ELISA development kits (R&D Systems) according to the manufacturer's instructions.

Bacterial killing assay. Bacterial killing assay was performed as described previously (54). Briefly, 0.1×10^6 CFU/ml *Escherichia coli* (BL21DE3pLysS) were added to macrophages in 96-well plates and incubated at 37°C for 1 hour. Supernatants were serially diluted and plated on Luria broth–agar plates. The plates were incubated overnight at 37°C, and bacterial colonies were counted. Data are presented as CFU/ml.

Real-time cell metabolism assay. An XF-24 Analyzer (Seahorse Bioscience) was used for recording of OCR. Briefly, BMDMs were seeded in Seahorse XF-24 microplates, and treated with or without 10 ng/ml IL-4 for 24 hours. Before analysis, the cells were incubated in OCR media for 1 hour at 37°C in room air. Cells were sequentially treated with 1.5 μg/ml oligomycin, 4.5 μM trifluoromethoxy carbonylcyanide phenylhydrazone (FCCP), and 1 μM antimycin plus 0.5 μM rotenone. Real-time OCR was recorded according to the manufacturer's manual.

ChIP assay. ChIP assays were performed as previously described (55). Briefly, BMDMs were fixed with 1% formaldehyde in PBS for 10 minutes and collected in RIPA buffer. Genomic DNA was then sheared by sonication to a length of approximately 200–500 bp. The extracts were incubated with anti-p65 antibody overnight, followed by precipitation with protein G agarose beads (Invitrogen). Genomic DNA in the immunocomplexes was purified using Qiagen miniprep columns (Qiagen). Primer sequences to specifically amplify the mouse *Malat1* promoter spanning the putative NF-κB binding site were sense, 5′-CATCTTGTTTCG-CATGAAATGGCA-3′ and antisense, 5′-TCCTGGGAGGACAGAGGGTATAGC-3′.

Statistics. One-way ANOVA followed by Bonferroni's test was used for multiple group comparisons. The 2-tailed Student's *t* test was used for comparison between 2 groups. $P < 0.05$ was considered statistically significant.

Study approval. Protocols for all experiments involving mice in this study were approved by the University of Alabama at Birmingham Institutional Animal Care and Use Committee (IACUC).

Author contributions

HC and GL designed the study. HC, SB, SG, NX, JG, DJ, and GL performed the experiments and/or analyzed the data. MZ provided critical materials. GL supervised the study. HC, VJT, and GL drafted the manuscript.

Acknowledgments

Address correspondence to: Gang Liu, Division of Pulmonary, Allergy, and Critical Care Medicine, Department of Medicine, University of Alabama at Birmingham, 901 19th St. So., BMR II 233, Birmingham, Alabama 35294, USA. Phone: 205.975.8932, Email: gangliu@uabmc.edu.

1. Lawrence T, Natoli G. Transcriptional regulation of macrophage polarization: enabling diversity with identity. *Nat Rev Immunol*. 2011;11(11):750–761.
2. Murray PJ, Wynn TA. Obstacles and opportunities for understanding macrophage polarization. *J Leukoc Biol*. 2011;89(4):557–563.
3. Mosser DM, Edwards JP. Exploring the full spectrum of macrophage activation. *Nat Rev Immunol*. 2008;8(12):958–969.
4. Sica A, Mantovani A. Macrophage plasticity and polarization: in vivo veritas. *J Clin Invest*. 2012;122(3):787–795.
5. Gordon S, Martinez FO. Alternative activation of macrophages: mechanism and functions. *Immunity*. 2010;32(5):593–604.
6. Mantovani A, Biswas SK, Galdiero MR, Sica A, Locati M. Macrophage plasticity and polarization in tissue repair and remodelling. *J Pathol*. 2013;229(2):176–185.
7. Tugal D, Liao X, Jain MK. Transcriptional control of macrophage polarization. *Arterioscler Thromb Vasc Biol*. 2013;33(6):1135–1144.
8. Murray PJ, et al. Macrophage activation and polarization: nomenclature and experimental guidelines. *Immunity*. 2014;41(1):14–20.
9. Ruffell B, Affara NI, Coussens LM. Differential macrophage programming in the tumor microenvironment. *Trends Immunol*. 2012;33(3):119–126.
10. Liu G, Abraham E. MicroRNAs in immune response and macrophage polarization. *Arterioscler Thromb Vasc Biol*. 2013;33(2):170–177.
11. Xie N, Liu G. ncRNA-regulated immune response and its role in inflammatory lung diseases. *Am J Physiol Lung Cell Mol Physiol*. 2015;309(10):L1076–L1087.
12. Arun G, et al. Differentiation of mammary tumors and reduction in metastasis upon Malat1 lncRNA loss. *Genes Dev*. 2016;30(1):34–51.
13. Gutschner T, et al. The noncoding RNA MALAT1 is a critical regulator of the metastasis phenotype of lung cancer cells. *Cancer Res*. 2013;73(3):1180–1189.
14. Sun Q, Hao Q, Prasanth KV. Nuclear long noncoding RNAs: Key regulators of gene expression. *Trends Genet*. 2018;34(2):142–157.
15. Michalik KM, et al. Long noncoding RNA MALAT1 regulates endothelial cell function and vessel growth. *Circ Res*. 2014;114(9):1389–1397.
16. Grünweller A, Wyszko E, Bieber B, Jahnel R, Erdmann VA, Kurreck J. Comparison of different antisense strategies in mammalian cells using locked nucleic acids, 2′-O-methyl RNA, phosphorothioates and small interfering RNA. *Nucleic Acids Res*. 2003;31(12):3185–3193.
17. Wilusz JE, Freier SM, Spector DL. 3′ end processing of a long nuclear-retained noncoding RNA yields a tRNA-like cytoplasmic RNA. *Cell*. 2008;135(5):919–932.
18. Gast M, et al. Long noncoding RNA MALAT1-derived mascRNA is involved in cardiovascular innate immunity. *J Mol Cell Biol*. 2016;8(2):178–181.
19. Gast M, et al. Immune system-mediated atherosclerosis caused by deficiency of long non-coding RNA MALAT1 in ApoE$^{-/-}$ mice. *Cardiovasc Res*. 2019;115(2):302–314.
20. Takeuchi O, Akira S. Pattern recognition receptors and inflammation. *Cell*. 2010;140(6):805–820.
21. Hakonarson H, et al. A genome-wide association study identifies KIAA0350 as a type 1 diabetes gene. *Nature*. 2007;448(7153):591–594.
22. Rubio JP, et al. Replication of KIAA0350, IL2RA, RPL5 and CD58 as multiple sclerosis susceptibility genes in Australians. *Genes Immun*. 2008;9(7):624–630.
23. Zoledziewska M, et al. Variation within the CLEC16A gene shows consistent disease association with both multiple sclerosis and type 1 diabetes in Sardinia. *Genes Immun*. 2009;10(1):15–17.
24. Australia New Zealand Multiple Sclerosis Genetics Consortium (ANZgene). Genome-wide association study identifies new multiple sclerosis susceptibility loci on chromosomes 12 and 20. *Nat Genet*. 2009;41(7):824–828.
25. Gateva V, et al. A large-scale replication study identifies TNIP1, PRDM1, JAZF1, UHRF1BP1 and IL10 as risk loci for systemic lupus erythematosus. *Nat Genet*. 2009;41(11):1228–1233.
26. Matthay MA, Ware LB, Zimmerman GA. The acute respiratory distress syndrome. *J Clin Invest*. 2012;122(8):2731–2740.

27. Huang SC, et al. Cell-intrinsic lysosomal lipolysis is essential for alternative activation of macrophages. *Nat Immunol*. 2014;15(9):846–855.

28. Jung SB, et al. Reduced oxidative capacity in macrophages results in systemic insulin resistance. *Nat Commun*. 2018;9(1):1551.

29. Huang SC, et al. Metabolic reprogramming mediated by the mTORC2-IRF4 signaling axis is essential for macrophage alternative activation. *Immunity*. 2016;45(4):817–830.

30. Tan Z, et al. Pyruvate dehydrogenase kinase 1 participates in macrophage polarization via regulating glucose metabolism. *J Immunol*. 2015;194(12):6082–6089.

31. Bricker DK, et al. A mitochondrial pyruvate carrier required for pyruvate uptake in yeast, Drosophila, and humans. *Science*. 2012;337(6090):96–100.

32. Xie N, et al. Metabolic characterization and RNA profiling reveal glycolytic dependence of profibrotic phenotype of alveolar macrophages in lung fibrosis. *Am J Physiol Lung Cell Mol Physiol*. 2017;313(5):L834–L844.

33. Burman A, Tanjore H, Blackwell TS. Endoplasmic reticulum stress in pulmonary fibrosis. *Matrix Biol*. 2018;68-69:355–365.

34. Vannella KM, Wynn TA. Mechanisms of organ injury and repair by macrophages. *Annu Rev Physiol*. 2017;79:593–617.

35. Du M, et al. The LPS-inducible lncRNA Mirt2 is a negative regulator of inflammation. *Nat Commun*. 2017;8(1):2049.

36. Sun D, et al. LncRNA GAS5 inhibits microglial M2 polarization and exacerbates demyelination. *EMBO Rep*. 2017;18(10):1801–1816.

37. Hirata H, et al. Long noncoding RNA MALAT1 promotes aggressive renal cell carcinoma through Ezh2 and interacts with miR-205. *Cancer Res*. 2015;75(7):1322–1331.

38. Pruszko M, et al. The mutant p53-ID4 complex controls VEGFA isoforms by recruiting lncRNA MALAT1. *EMBO Rep*. 2017;18(8):1331–1351.

39. Tripathi V, et al. The nuclear-retained noncoding RNA MALAT1 regulates alternative splicing by modulating SR splicing factor phosphorylation. *Mol Cell*. 2010;39(6):925–938.

40. Bernard D, et al. A long nuclear-retained non-coding RNA regulates synaptogenesis by modulating gene expression. *EMBO J*. 2010;29(18):3082–3093.

41. Xiao X, et al. LncRNA MALAT1 sponges miR-204 to promote osteoblast differentiation of human aortic valve interstitial cells through up-regulating Smad4. *Int J Cardiol*. 2017;243:404–412.

42. Soleimanpour SA, et al. The diabetes susceptibility gene Clec16a regulates mitophagy. *Cell*. 2014;157(7):1577–1590.

43. Schuster C, et al. The autoimmunity-associated gene CLEC16A modulates thymic epithelial cell autophagy and alters T cell selection. *Immunity*. 2015;42(5):942–952.

44. Dambuza IM, Brown GD. C-type lectins in immunity: recent developments. *Curr Opin Immunol*. 2015;32:21–27.

45. Cummings RD, and McEver RP. C-type lectins. In: Varki A, et al. eds. *Essentials of Glycobiology*. Cold Spring Harbor, NY: 2009.

46. Gause WC, Wynn TA, Allen JE. Type 2 immunity and wound healing: evolutionary refinement of adaptive immunity by helminths. *Nat Rev Immunol*. 2013;13(8):607–614.

47. Eißmann M, et al. Loss of the abundant nuclear non-coding RNA MALAT1 is compatible with life and development. *RNA Biol*. 2012;9(8):1076–1087.

48. Banerjee S, et al. MicroRNA let-7c regulates macrophage polarization. *J Immunol*. 2013;190(12):6542–6549.

49. Misharin AV, Morales-Nebreda L, Mutlu GM, Budinger GR, Perlman H. Flow cytometric analysis of macrophages and dendritic cell subsets in the mouse lung. *Am J Respir Cell Mol Biol*. 2013;49(4):503–510.

50. McCubbrey AL, et al. Deletion of c-FLIP from CD11bhi macrophages prevents development of bleomycin-induced lung fibrosis. *Am J Respir Cell Mol Biol*. 2018;58(1):66–78.

51. Liu G, et al. miR-21 mediates fibrogenic activation of pulmonary fibroblasts and lung fibrosis. *J Exp Med*. 2010;207(8):1589–1597.

52. Yang S, et al. Participation of miR-200 in pulmonary fibrosis. *Am J Pathol*. 2012;180(2):484–493.

53. Liu G, Park YJ, Abraham E. Interleukin-1 receptor-associated kinase (IRAK) -1-mediated NF-kappaB activation requires cytosolic and nuclear activity. *FASEB J*. 2008;22(7):2285–2296.

54. Cui H, Banerjee S, Guo S, Xie N, Liu G. IFN regulatory factor 2 inhibits expression of glycolytic genes and lipopolysaccharide-induced proinflammatory responses in macrophages. *J Immunol*. 2018;200(9):3218–3230.

55. Cui H, et al. The human long noncoding RNA lnc-IL7R regulates the inflammatory response. *Eur J Immunol*. 2014;44(7):2085–2095.